

ARTICLE OPEN



Soft, stretchable thermal protective substrates for wearable electronics

Shuang Nie^{1,2}, Min Cai², Huang Yang³, Liyin Shen³, Suhao Wang^{1,2}, Yang Zhu³✉ and Jizhou Song^{1,2,4}✉

Wearable electronics have continued to attract the attention of researchers and clinicians due to their great potential in medical applications. During their operations, the undesired heating may cause thermal discomfort or damage to skin. Seeking materials and structures for advanced thermal protection has become an urgent issue. Here, we report a soft, stretchable thermal protective substrate for wearable electronics with remarkable thermal insulating performance, mechanical compliance and stretchability. The thermal protective substrate features a composite design of the widely used polymeric material polydimethylsiloxane with embedded heat absorbing microspheres, consisting of phase change materials encapsulated inside the resin shell. Experimental and numerical studies show that the thermal protective substrate could be subjected to complex deformations over 150% and could reduce the peak skin temperature increase by 82% or higher under optimizations. In vivo demonstration of this concept on the mouse skin illustrates its unusual thermal protection capability for wearable thermal management.

npj Flexible Electronics (2022)6:36; <https://doi.org/10.1038/s41528-022-00174-8>

INTRODUCTION

Wearable electronics have continued to attract the attention of researchers and clinicians due to their ability to have a conformal contact to skin with great potential in medical applications such as healthcare monitoring^{1–3}, wound management^{4,5}, and drug release^{6,7}. In the past decade, considerable efforts have been dedicated to develop high-performance wearable electronic devices by integrating functional components onto the soft polymer substrate via advanced manufacturing technologies^{8–11} for continuous and accurate measurement of human vital signs^{12–20}. Among these successful demonstrations, many involve functional heating components (e.g., light-emitting-diode), which extremely require advanced thermal management techniques to protect the skin from undesired heating due to the low heat insulating performance of commonly used soft polymer substrates such as polydimethylsiloxane (PDMS) and ecoflex. To enhance the thermal insulating capability of a substrate, insulation fillers (e.g., hollow microspheres, aerogel) with low thermal conductivities^{21,22} or phase change materials (e.g., paraffin wax, polyethylene glycol) with abilities to absorb and release large amounts of latent heat energy at a constant transition temperature^{23–27} have been extensively utilized for thermal management of electronic devices. Despite the notable advances, the solid rigidity or liquid leakage associated with the above composite designs makes them unsuitable for wearable thermal management. Recent attempts based on orthotropic substrate design²⁸ and functional soft composite design²⁹ by controlling the heat flow direction have shown great promise for the thermal management of wearable electronics. However, the compromise of flexibility and stretchability greatly limits their broad utilities in practical applications. Thus, the design of a soft, stretchable thermal protective substrate for thermal protection of skin remains a challenge for wearable thermal management.

Here, we report a soft, stretchable thermal protective substrate for wearable thermal management with capabilities to provide thermal protection to skin while maintaining softness and stretchability to ensure intimate contact with skin. The thermal protective substrate features a composite design of the widely-used polymeric material polydimethylsiloxane (PDMS) with embedded heat-absorbing microspheres, which consist of phase change material (n-icosane) encapsulated inside the melamine-formaldehyde resin shell. The encapsulation shell not only avoids the leakage of phase change material when it experiences solid-liquid phase transition to absorb large amounts of heat energy but also reacts with the platinum catalyst³⁰ to prevent the cross-linking reaction, yielding a desired soft, stretchable, and adhesive substrate. The proposed composite design overcomes the challenges of solid rigidity and liquid leakage associated with existing designs and offers a suitable route to develop a soft, stretchable thermal protective substrate for wearable thermal management. Experimental and numerical studies have been carried out to reveal the fundamental aspects of the design, fabrication, and operation of the thermal protective substrate with remarkable thermal insulating performance, mechanical compliance, and stretchability. In vivo demonstration of this concept in a wearable heater on the mouse skin illustrates its unusual thermal protection capability for wearable thermal management.

RESULTS AND DISCUSSION

Design of the thermal protective substrate

Figure 1a–c schematically shows the concept of the proposed thermal protective substrate (TPS) with the capabilities of thermal insulation, mechanical compliance, and stretchability, which are highly desirable in practical applications of wearable electronic devices bonding to skin. Heat-absorbing microspheres with phase

¹Department of Rehabilitation Medicine, The First Affiliated Hospital College of Medicine, Zhejiang University, Hangzhou 310027, China. ²Department of Engineering Mechanics, Soft Matter Research Center, and Key Laboratory of Soft Machines and Smart Devices of Zhejiang Province, Zhejiang University, Hangzhou 310027, China. ³MOE Key Laboratory of Macromolecular Synthesis and Functionalization, Department of Polymer Science and Engineering, Zhejiang University, Hangzhou 310027, China. ⁴State Key Laboratory of Fluid Power and Mechatronic Systems, Zhejiang University, Hangzhou 310003, China. ✉email: zhuyang@zju.edu.cn; jzsong@zju.edu.cn

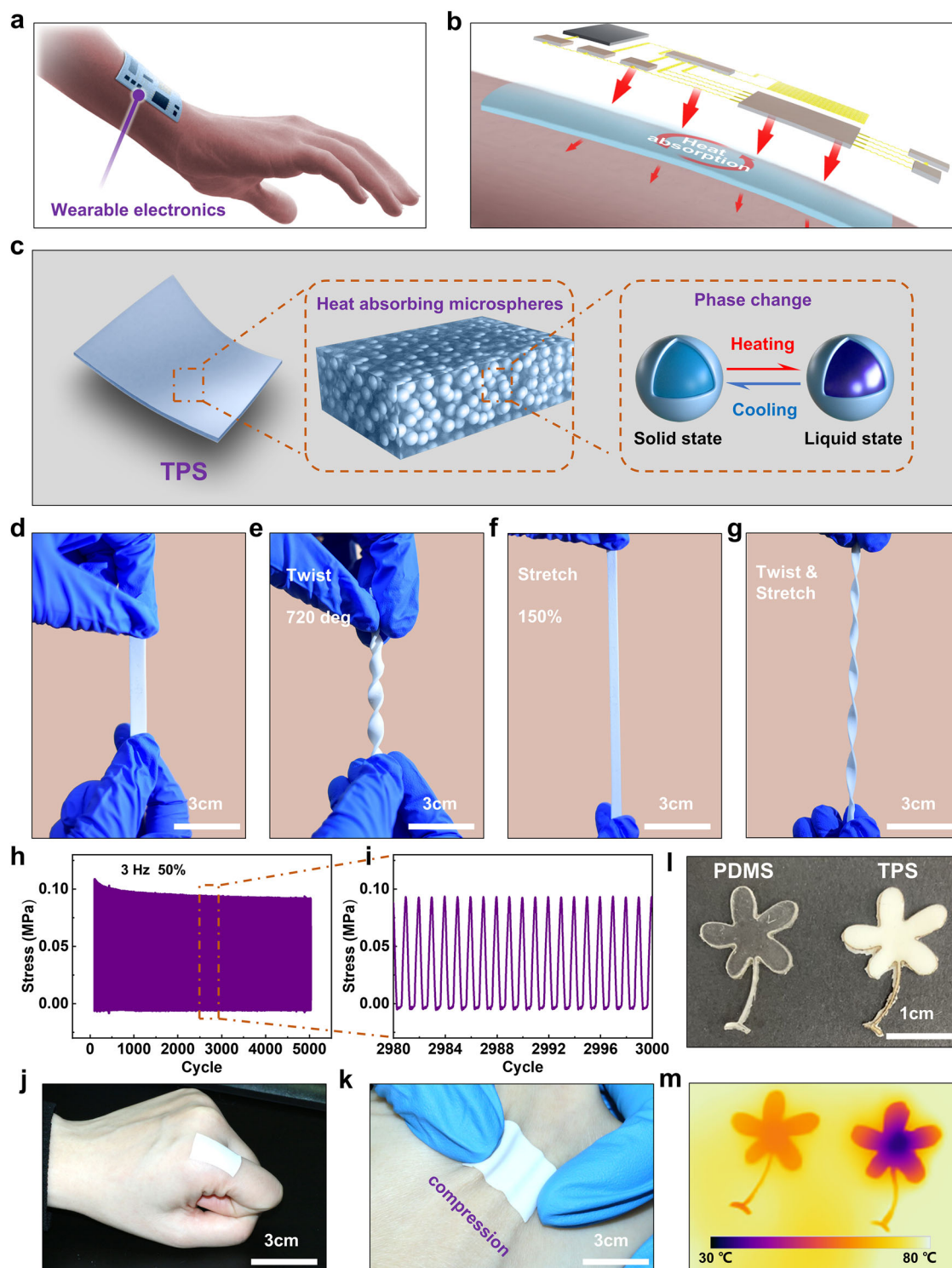


Fig. 1 Design concept and illustrations of the proposed thermal protective substrate (TPS) for wearable electronics with the capabilities of thermal insulation, mechanical compliance, and stretchability. **a** Schematic illustration of a wearable electronic device attached to human skin. **b** Schematic illustration of heat transfer from devices to skin with the TPS absorbing large amounts of heat energy. **c** Schematic illustration of TPS composed of a polymer matrix embedded by heat-absorbing microspheres consisting of phase change materials encapsulated by the resin shell. The solid-liquid phase change occurs during the heating and cooling processes. Optical images of TPS under various deformations: **d** undeformed, **e** twist, **f** stretch, and **g** twist/stretch. **h, i** Cyclic loading test of TPS under an applied strain of 50% at a frequency of 3 Hz. **j** TPS attached to the index finger joint with stretch. **k** TPS attached to the index finger joint with compression. **l** Optical image of PDMS and TPS without heating. **m** Thermal image of PDMS and TPS after placed on 80 °C hot plate for 10 s. The TPS is composed of heat-absorbing microspheres with a mass ratio of 80%.

change material of n-eicosane encapsulated inside a polymer shell of melamine-formaldehyde resin are adopted to mix with the commonly used polymer PDMS to enable the thermal insulation ability. During device operation, large amounts of heat energy generated from the functional heating component are absorbed by the solid-liquid phase change of n-eicosane to avoid excessive heating of skin (Fig. 1b, c). Thus, the temperature at the substrate/skin interface could be much lower than that of the heat source. Different from existing phase change material-enabled thermal protective substrate designs without required mechanical compliance and stretchability for a reliable skin/device interface, the proposed design introduces an appealing cross-linking inhibition process³⁰ due to the melamine-formaldehyde resin shell of phase change microsphere to yield a desirable soft, stretchable composite substrate.

To demonstrate the benefits of the proposed TPS, we mixed the heat-absorbing microspheres (phase change temperature: $\sim 37^\circ\text{C}$, GreenTech LF) with the liquid PDMS (Sylgard 184, 10:1 mass ratio of base to curing agent, Dow Corning) with the mass ratio varying from 0 to 80%. It should be noted that there are several other phase change materials with higher latent heat such as palmitic acid³¹, myristic acid³², and pentaglycine³³. Although these materials may absorb more heat energy during operation, the phase change temperature, which is usually above 55°C , is so high that induces thermal damage to biological tissue. To be a good material candidate for the thermal protective substrate of wearable thermal management, the phase change material embedded in the substrate should satisfy several constraints. The bottom requirement is that the phase change temperature should be higher than the core body temperature ($\sim 37^\circ\text{C}$)³⁴ and lower than the temperature ($\sim 43^\circ\text{C}$)³⁵ above which causes thermal discomfort. Moreover, the more the latent heat, the better the thermal insulating performance. The current phase change material has a phase change temperature just above the core body temperature, which serves as a very good candidate for wearable thermal management despite that it may not have the highest latent heat.

The fabrication of TPS is simple and only involves stirring, molding, and baking processes, as illustrated in Supplementary Fig. 1a. More details are given in the Methods section. The diameter of heat-absorbing microspheres is on the order of $30\ \mu\text{m}$ (Supplementary Fig. 1b), which indicates the limit of TPS thickness. Figure 1d–k demonstrate the mechanical compliance and stretchability of TPS with 80 wt% heat-absorbing microspheres. Unlike existing composites by physically blending phase change materials with compliant polymers with undesired increased stiffness and decreased stretchability, the proposed TPS is very soft due to the chemical inhibition of cross-linking, and could be subjected to complex deformations (such as stretch, twist, stretch/twist) over 150% without failures (Fig. 1d–i). To evaluate the mechanical stability of TPS, a fatigue test by the fatigue machine (M200, CARE) with a large strain (50%) at 3 Hz frequency for 5000 times was carried out. The output of stress was recorded in Fig. 1h with the middle 20 cycles plotted in Fig. 1i. The maximum stress remains almost unchanged during the 5000 loading/unloading cycles, which indicates a good elasticity of the proposed TPS. The reaction of polymer shell of heat-absorbing microspheres with platinum catalyst³⁰ which prevents the cross-linking of PDMS base and curing agent, significantly enhances the mechanical compliance of TPS and helps the adhesion of TPS to skin. Figure 1j, k show TPS conformally attached to the index finger joint and the opisthenar subjected to stretch and compression, which indicates a great adhesion of TPS.

To demonstrate the remarkable heat insulating performance of TPS, we cut the commonly used PDMS substrate and the proposed TPS with a mass ratio of 80% of heat-absorbing microspheres into flower shapes (thickness: 1 mm) as shown in Fig. 1l and placed them on an 80°C hot plate for 10 s with the temperature changes recorded by a thermal imager. The heat flux

conducting through the substrate from the hot plate will cause a temperature rise on the top surface. Due to the heat-absorbing microspheres, which absorb large amounts of heat energy during the heat transfer, the thermal insulating performance of TPS has been significantly improved compared to that of PDMS substrate. As shown in Fig. 1m, the maximum surface temperature of TPS is only 53°C with the most regions below 50°C , while that of PDMS substrate can reach as high as 68°C almost uniformly. To demonstrate the heat insulating performance of TPS over multiple heating cycles, the TPS with a mass ratio of 80% heat-absorbing microspheres (thickness 1.3 mm) was placed on a 70°C hot plate for 40 s followed by cooling it to room temperature and reheating it again. It is observed that the maximum surface temperature remains almost unchanged over 50 heating cycles (Supplementary Fig. 2), which indicates that the proposed TPS has a stable heat insulating performance.

Mechanical and thermal properties of thermal protective substrates

Systematic experimental studies were carried out to investigate the mechanical and thermal properties of TPS. Figure 2a shows the elastic modulus of TPS as the function of the mass ratio of heat-absorbing microspheres at various temperatures of 20, 50, and 100°C . The temperature, no matter it is higher or lower than the phase transition temperature ($\sim 37^\circ\text{C}$), has a negligible influence on the elastic modulus although a higher temperature may slightly increase the modulus at low mass fractions. As the mass ratio increases, the TPS becomes softer due to the cross-linking inhibition reaction between the melamine-formaldehyde resin shell and platinum catalyst³⁰. It is shown that the elastic modulus could decrease 98% from 1.56 to 0.023 MPa when the mass ratio increases from 0 to 80%. Figure 2b gives the maximum tensile strain as the function of the mass ratio of heat-absorbing microspheres at different temperatures. The temperature has a notable influence on the maximum tensile strain. Although the increase in temperature causes a decrease in the maximum tensile strain, the TPS still can be stretched over 100% even if the temperature is higher than 100°C . The maximum tensile strain of TPS shows an overall slightly increasing trend with the increase of a mass fraction of heat-absorbing microspheres. For example, when the mass ratio increases from 0 to 80%, the maximum tensile strain of TPS increases only 16.3 from 194.3% to 226.1% at a temperature of 25°C before phase change occurs and only 15.5% from 157.6 to 182.1% at a temperature of 100°C after phase change occurs. These results indicate that the addition of heat-absorbing microspheres to PDMS yields a low density of cross-linking due to the cross-linking inhibition reaction, which makes the TPS more compliant and stretchable at the break. The above feature is highly desirable in wearable thermal management but not for other applications requiring the maximization of the loading of filler materials. Although PDMS is a widely-used elastomer, its chemical cross-linking requirement based on Pt catalysts sometimes hinders a large loading of the filler material. Since the loading amounts of microspheres is sensitive to the heat absorption amount, the efforts to maximize the loading amount is also meaningful as demonstrated in thermoplastic elastomers such as poly(styrene-butadiene-styrene) (SBS)³⁶ and poly(styrene-ethylene-butylene-styrene) (SEBS)³⁷ instead of the chemically-crosslinked elastomers (e.g., PDMS). Figure 2c shows the dependence of TPS density on the mass ratio of heat-absorbing microspheres, which clearly indicates that the density remains almost a constant at $970\ \text{g cm}^{-3}$.

The thermal properties of TPS are important to optimize thermal insulating performance. The high-temperature synchronous thermal analyzer (NETZSCH DSC 214, Germany) was utilized to measure the thermal conductivity and specific heat capacity of TPS. The thermal conductivities before and after phase change,

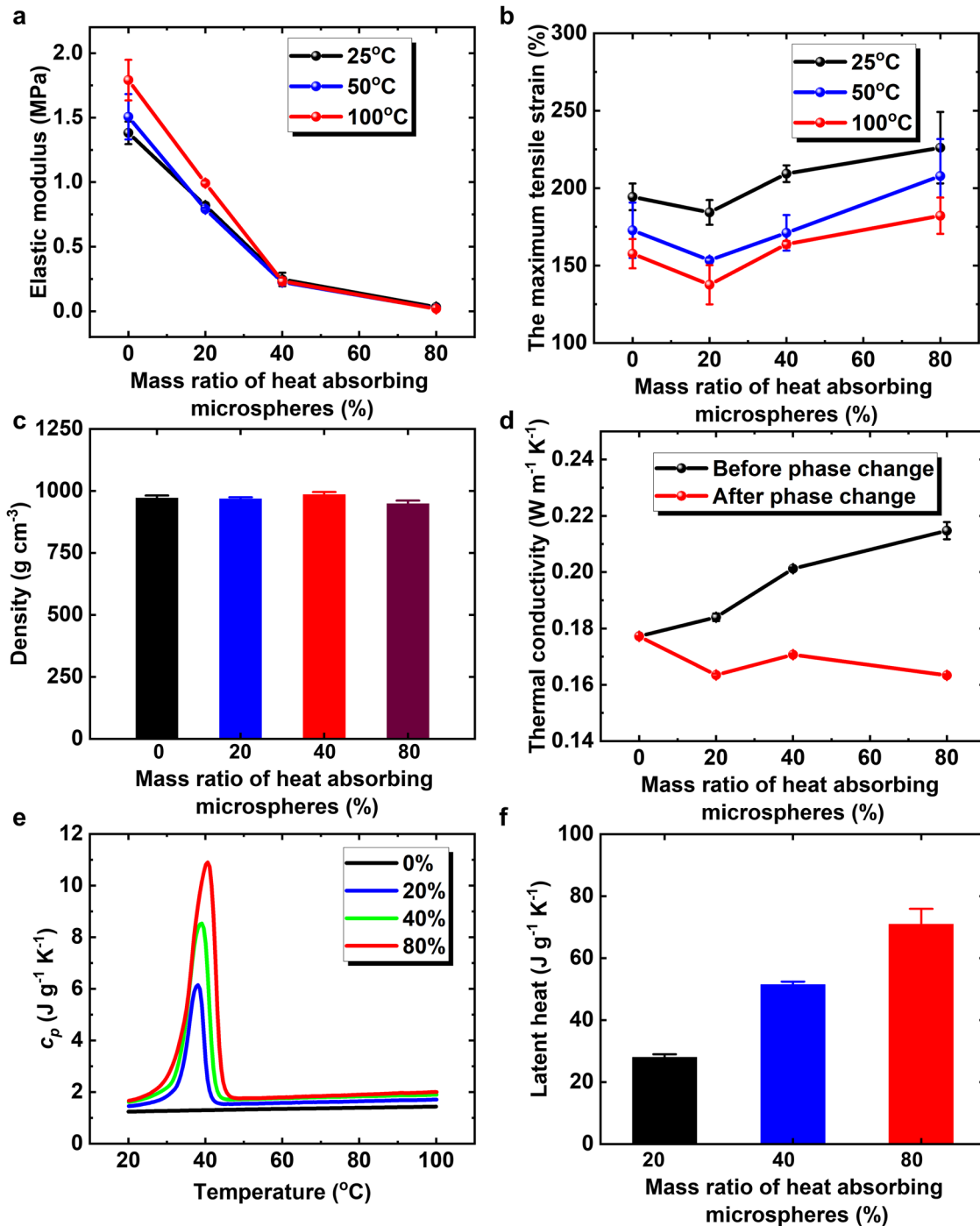


Fig. 2 Mechanical and thermal properties of TPS. **a** The elastic modulus of TPS and **b** the maximum tensile strain of TPS versus the mass ratio of heat-absorbing microspheres under different temperatures. **c** The density of TPS versus the mass ratio of heat-absorbing microspheres. **d** The thermal conductivity of TPS versus the mass ratio of heat-absorbing microspheres before and after the phase change (50 °C). **e** The variation of the specific heat capacity of TPS with temperature under different mass ratios of heat-absorbing microspheres. **f** The latent heat of TPS versus the mass ratio of heat-absorbing microspheres.

corresponding to temperatures of 25 and 50 °C, respectively, as functions of the mass ratio of heat-absorbing microspheres are given in Fig. 2d. Before the phase transition, the thermal conductivity of TPS is higher than that of PDMS and increases from 0.177 to 0.218 W m⁻¹ K⁻¹ with the increase of mass ratio from 0 to 80%. After the phase transition, the thermal conductivity of TPS is lower than that of PDMS and decreases slightly from 0.177 to 0.163 W m⁻¹ K⁻¹ with the increase of mass ratio from 0 to

80%. These opposite trends in thermal conductivity of TPS before and after the phase transition may be contributed to the change of thermal conductivity of heat-absorbing microspheres. Before the phase transition, the thermal conductivity of the heat-absorbing microspheres is higher than that of PDMS, and therefore, the thermal conductivity of TPS increases as the mass ratio of the heat-absorbing microspheres increases. After the phase transition, the phase change materials inside the heat-

absorbing microspheres undergo a phase change and the thermal conductivity of the heat-absorbing microspheres becomes slightly lower than that of PDMS. Thus, the thermal conductivity of TPS decreases slightly as the mass ratio of the heat-absorbing microspheres increases. Figure 2e shows the variation of the specific heat capacity of TPS with the temperature under different mass ratios of heat-absorbing microspheres. The specific heat capacity of PDMS, corresponding to the mass ratio of 0%, remains almost a constant at $1.35 \text{ J g}^{-1} \text{ K}^{-1}$, which indicates that no phase transition occurs and the latent heat is zero. However, the specific heat capacity of TPS has an obvious endothermic peak at around 37°C , which is the same as the phase transition temperature of the embedded heat-absorbing microspheres. As expected, the peak value of specific heat capacity increases with the increase of mass ratio since a higher mass ratio involves more phase change materials, leading to a larger latent heat. As illustrated in Fig. 2f, the latent heat of TPS linearly depends on the mass ratio of heat-absorbing microspheres. These results provide the material foundation for designing TPS to achieve the desired thermal insulating performance for wearable thermal management.

Thermal insulating performance of thermal protective substrates

To demonstrate the thermal insulating effect, we developed a wearable electronic device with a heater (10 mm diameter, 20- μm thickness, shown in Supplementary Fig. 3) as the heating source on the TPS with a diameter of 20 mm. The ambient temperature is 29°C . Figure 3a shows the schematic illustration of the device with a TPS thickness of 1.4 mm. The heat flux passing through the substrate causes the increase in skin temperature with the maximum value occurring on the bottom surface of the device (or top surface of the skin) during its operation. Here, an infrared thermal imager was used to measure the maximum temperature (without skin) at the bottom surface to quantify the thermal insulating performance of TPS. Finite element analysis (FEA) was also carried out to investigate the thermal protective effect of TPS with details given in the Methods section. The temperature distributions on the bottom surface of a substrate at the heating time of 75 s are shown in Fig. 3a with the heating power of 140 mW. FEA results agree well with experimental measurements, which indicates that FEA is valid and accurate to predict temperatures in the system.

To understand the thermal protection mechanism of TPS, we compared the maximum temperature on the bottom surface of the substrate when the mass ratio of heat-absorbing microspheres varies from 0 to 80% during the device operation (heating power: 140 mW) in Fig. 3b. For the wearable electronic device with a PDMS substrate, corresponding to a mass ratio of 0%, the maximum temperature increases monotonically and continuously to a stable temperature of around 59.5°C . At first, the maximum temperature rises rapidly and then the rise rate decreases until the temperature becomes stable. However, for the wearable electronic device with a TPS, the thermal response is more complicated and can be described by two distinct stages. In the first stage with the temperature below a value slightly lower than the phase transition temperature, the maximum temperature rises slowly for a period of time, yielding a much lower temperature compared with the case of PDMS substrate. The reason is that the heat-absorbing microspheres experience the solid-liquid phase transition to absorb large amounts of excess heat energy. Moreover, the larger the mass ratio of heat-absorbing microspheres, the lower the maximum temperature. Once the phase transition completes, the maximum temperature reaches the second stage with a similar temperature rise rate as the case of PDMS substrate. It is shown that the maximum temperature at the steady-state decreases slightly as the mass ratio of heat-absorbing microspheres increases. For example, the steady maximum temperature drops

only from 59.5 to 55.3°C with the increase of mass ratio from 0 to 80%.

It is obvious that the maximum temperature depends on the heating duration time. Considering that the phase transition completes at around 75 s for the mass ratio of 80%, which is the case with the best thermal insulating performance. The evolutions of the maximum temperature with the heating duration time of 75 s are shown in Fig. 3c with various mass ratios of heat-absorbing microspheres. The material and geometrical parameters are the same as those in Fig. 3b. The good agreement between experimental measurements and FEA again validates the accuracy of FEA. It is clearly shown that the maximum temperature decreases significantly during the heating process with the increase of the mass ratio of heat-absorbing microspheres. The maximum temperature on the bottom surface of the substrate can reach a peak value of 51°C for the wearable electronic device with a PDMS substrate, while those for the wearable electronic devices with thermal protective substrates reach only 47, 41, and 33°C for the mass ratios of 20, 40, and 80%, respectively. To quantify the thermal insulation performance of TPS, we define the percentage of temperature reduction as the relative peak temperature difference for the cases with PDMS substrate and TPS over the temperature increase of the case with PDMS substrate. The temperature reduction percentages are 18, 45, and 82% for the mass ratios of 20, 40, and 80%, respectively, which clearly indicate that the proposed TPS has much better thermal insulating performance than the conventional PDMS substrate and can serve as the thermal protective substrate for wearable electronic devices. When the wearable electronic device does not operate, the maximum temperature cools down and finally reaches the ambient temperature after a long period of time. Considering that the TPS absorbs large amounts of heat energy during the heating process, the maximum temperature for the case of TPS drops much slower than that of PDMS substrate during the cooling process due to the liquid-solid phase transition.

To better understand the thermal behaviors of wearable electronic devices with TPS, the influences of substrate thickness, heating powers, and external stretch on the maximum temperature are systematically investigated. The heating duration time and mass ratio of heat-absorbing microspheres are set as 75 s and 80%, respectively. Figure 3d shows the maximum temperature on the bottom surface of the substrate as the function of time with various TPS thicknesses of 0.8, 1.0, and 1.4 mm. The heating power is set as 140 mW. According to Fig. 3b, the case of 1.4 mm contains just enough phase change materials to absorb the excessive heat energy. The phase transition could occur during the whole heating process, thus yielding the lowest peak value of the maximum temperature. While for the cases of 0.8 and 1.0 mm, the phase change materials in TPS are not enough and the phase transition could complete before the unheating process starts, thus yielding much higher peak values of the maximum temperature. The temperature distribution on the bottom surface of a substrate at the time of 75 s with different thicknesses (Supplementary Fig. 4) also indicates that the smaller the substrate thickness, the higher the peak value of the maximum temperature. Figure 3e shows the maximum temperature on the bottom surface of TPS as the function of time with various heating powers of 140, 210, and 270 mW. The TPS thickness is set as 1.4 mm. Considering that the TPS contains just enough phase change materials to absorb the excessive heat energy under a heating power of 140 mW (Fig. 3b), more heat energies under higher heating powers will enter the system and yield much higher peak values of the maximum temperature. The temperature distribution on the bottom surface of TPS at the time of 75 s with different heating powers (Supplementary Fig. 5) also indicates that the higher the heating power, the higher the peak value of the maximum temperature. Supplementary Fig. 6 shows the temperature distributions on the bottom surface of TPS (mass ratio:

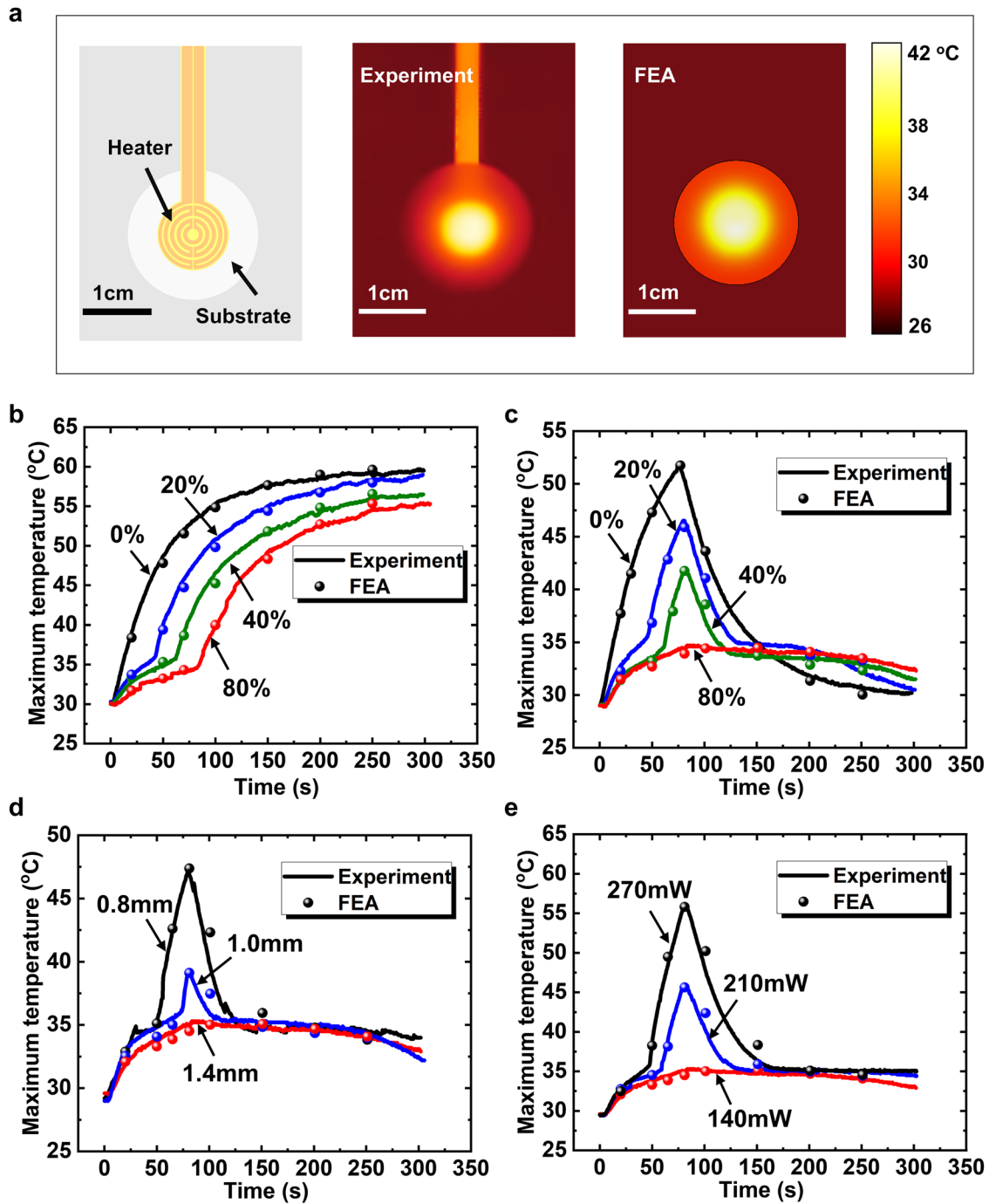


Fig. 3 Thermal insulating performance of TPS. **a** Schematic illustration of a wearable heater on a TPS (left), the thermal image of the bottom surface of TPS by experiment (middle) and the temperature distribution on the bottom surface of TPS by FEA (right). The evolution of the maximum temperature on the bottom surface of TPS (thickness: 1.4 mm) with different mass ratios of heat-absorbing microspheres under a heating power of 140 mW with **b** the heating duration of 300 s, and **c** the heating duration of 75 s. **d** The influence of TPS thickness on the maximum temperature (heating power: 140 mW, heating duration: 75 s). **e** The influence of heating power on the maximum temperature (TPS thickness: 1.4 mm, heating duration: 75 s).

80%, thickness: 1.3 mm) at the time of 75 s with different tensile strains (0, 30, 50, 80%) under a heating power of 140 mW. There is no apparent difference in the peak value of the maximum temperature, which indicates that the external stretch has a negligible influence on the thermal insulating performance. These results provide important guidelines for the design of TPS to achieve the desired thermal insulating performance.

In vivo experiment of skin protection

Depilated mice are used to characterize the thermal protective ability of TPS as shown in Fig. 4a. The heater operates for 40 s at the heating power of 445 mW and then stops heating for 140 s. For comparison, the thermal protection effects of wearable electronic devices with conventional PDMS substrate and the proposed TPS are both investigated. The substrate thickness is

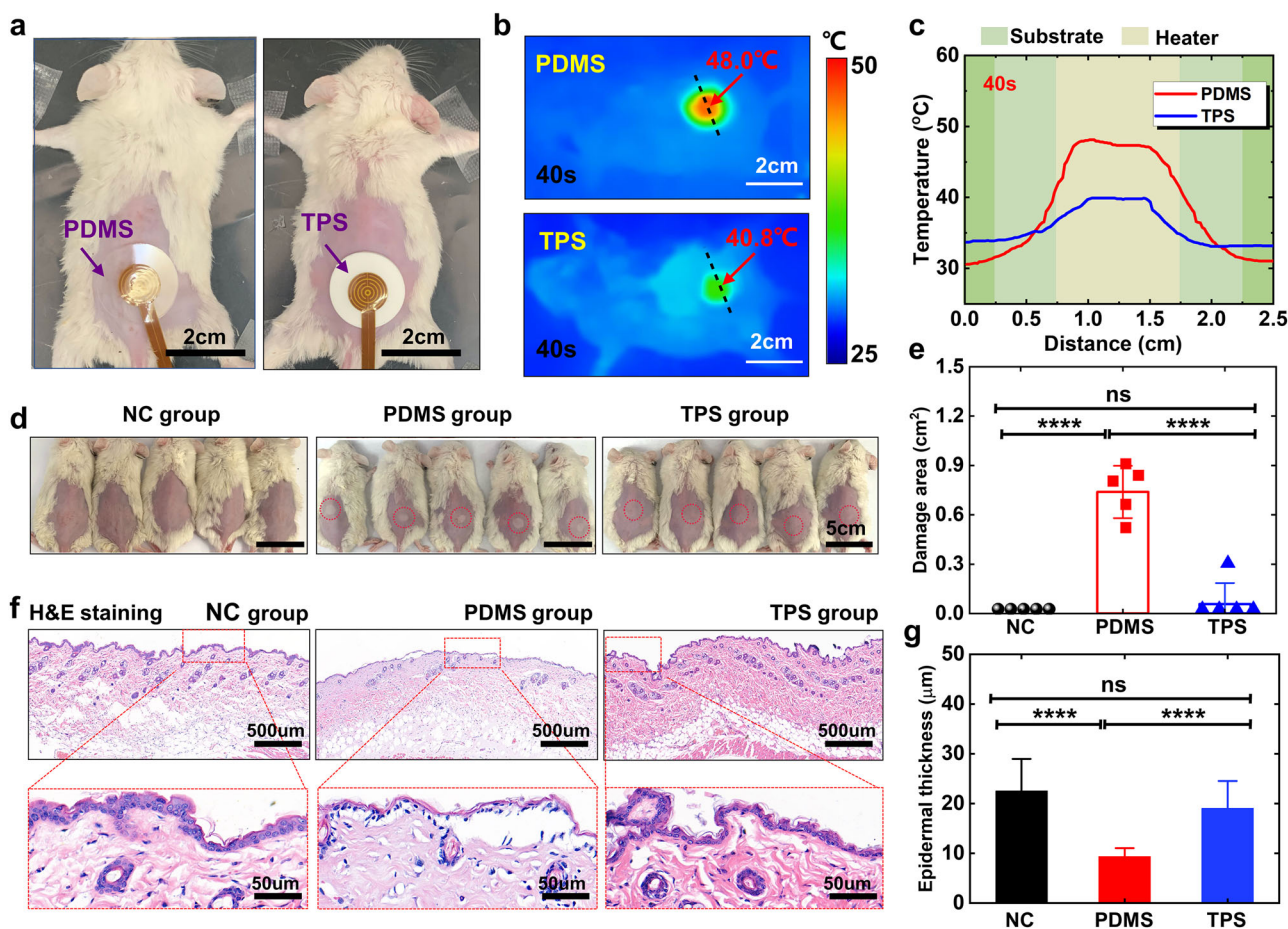


Fig. 4 Animal experiment of thermal protection for the skin. **a** Photos of wearable heaters with the PDMS substrate (left) and TPS (right) attached to the mice skin. **b** Thermal images of the mice skin after heating for 40 s. **c** The temperature change along the dotted line in Fig. 4b. **d** Photos of mice after experimenting in NC (left), PDMS (middle), and TPS (right) group. **e** The area of damaged skin in NC, PDMS, and TPS group. **f** Hematoxylin-eosin (H&E) staining of mice skin in NC (left), PDMS (middle), and TPS (right) group. **g** The epidermal thickness in NC, PDMS, and TPS group. The thickness of the substrate is 1.3 mm and the heating power is 445 mW.

1.3 mm. After heating for 40 s, the maximum temperature of the skin surface of the PDMS group is 48.0 °C (Fig. 4b), while that of TPS is only 40.8 °C recorded by the infrared thermal imaging camera. Along the black dotted line (Fig. 4b), the skin surface temperature for the case of PDMS substrate remains much higher than that of TPS in the central area (i.e., the area under the heater) as shown in Fig. 4c even though the body temperature of the TPS group is higher than that of PDMS group. Meanwhile, the skin temperature gradually decreased in the area far away from the heater. These results clearly show the outstanding thermal protective ability of TPS for the skin. After turning off the heater for 140 s, the highest temperature of mice skin in TPS is 34.8 °C, while that in the PDMS group is still as high as 39.0 °C (Supplementary Fig. 7a, b).

After the animal experiment, obvious blisters could be observed in all mice of the PDMS group, while only slight blisters could be found in the TPS group as shown in Fig. 4d. At the same time, the average damaged skin area in the TPS group is 0.057 cm², which is significantly less than that in the PDMS group (0.739 cm²), which shows that TPS has a much better protective ability to skin (Fig. 4e). Hematoxylin-eosin (H&E) staining (Fig. 4f) is used to characterize the morphology of the skin. It could be found that some cutaneous appendages disappeared and the epidermis fell off in the PDMS group, while its morphology maintained completely in the TPS group. The thickness of the epidermis is further counted to evaluate the surface injury. As shown in Fig. 4g, the thickness in the PDMS group is 9.36 µm, which is much lower

than Normal Control (NC) group (22.54 µm). With the doping of heat-absorbing microspheres, the epidermis thickness in the TPS group is 19.05 µm and shows a slight decrease. The above results indicate that the proposed TPS can improve thermal insulation performance substantially.

In this study, we proposed a soft, thermal protective substrate for wearable electronic devices. The thermal protective substrate features heat-absorbing microspheres, consisting of phase change materials encapsulated by a resin shell, embedded in the widely-used polymeric material PDMS. Mechanical and thermal properties of the thermal protective substrate have been systematically investigated. It is shown that the thermal protective substrate has remarkable thermal insulating performance, mechanical compliance, and stretchability. The phase transition of phase change materials contributes to the ability of thermal insulation, while the chemical prohibition of cross-linking of resin shells contributes to the desired increased compliance and stretchability for better conformal contact to the skin. Compared with the conventional PDMS substrate, the thermal protective substrate could reduce the peak skin temperature increase by 82% or even higher under optimizations. In vivo demonstration of this concept in a wearable heater on depilated mice illustrates its unusual thermal protection capability for wearable thermal management. Despite the attractive thermal insulating performance, mechanical compliance, and large stretchability, the thermal protective substrate still needs improvements in some aspects. For example, the white heat-absorbing microspheres make the substrate milky white,

which may limit its broad utilities in applications requiring transparent substrates.

METHODS

Fabrication of the thermal protective substrate

The fabrication of thermal protective substrate is simple and only involves stirring, molding, and baking processes, as illustrated in Supplementary Fig. 1a. PDMS (Sylgard 184, Dow Corning) mixture was prepared by mixing the base and curing agent in a 10:1 mass ratio. Then, the heat-absorbing microspheres (phase change temperature: $\sim 37^\circ\text{C}$, diameter: $\sim 30\ \mu\text{m}$, GreenTech LF) were mixed with the liquid PDMS with the mass ratio varying from 0 to 80%. The mixture was then added to a mold followed by degassing for 30 min and then curing in an oven at 85°C for 3 h, 99°C for 3 h, and 115°C for 12 h. Due to the fluidity of the mixture of heat-absorbing microspheres and liquid PDMS, spin-coating can be used to fabricate a thin film of TPS for encapsulation or additional substrate layer with easily controlled uniformity and thickness in practical applications. Although the thermal protective substrate is not compatible with the conventional microfabrication processes, a pattern (e.g., kirigami pattern) can be easily achieved by screen printing for more interesting applications.

Finite element analysis

A 3D thermal model is established in COMSOL. Due to the thin thickness of the heater, the heater is modeled as a surface heat source. The free surfaces have natural convection boundaries with the coefficient of natural convection of $14\ \text{W m}^{-2}\ \text{K}^{-1}$. The ambient temperature is 29°C . The thermal conductivity, density, and specific heat of PDMS substrate and thermal protective substrate have been measured in Fig. 2c–e. The phase changes the temperature of the thermal protective substrate is set as 37°C with the latent heat given in Fig. 2f. The element size ranges from 0.0315 to 0.735 mm with a total number of over 25,000. The fine mesh is adopted for the region near the heat source and the coarse mesh for that far from the heat source. The convergence of FEA has been verified by the tiny change of less than 0.1% via the comparison with a model using a much smaller element size of 0.01 mm.

Animal experiment

The ICR mice were depilated and randomly divided into three groups ($n = 5$): (1) Negative control group (NC group, without any operation); (2) PDMS group (PDMS as thermal protective substrates); (3) TPS group (TPS as thermal protective substrates). After being attached to the skin surface, the heater was turned on for 40 s at the power of 445 mW and then turned off for 140 s. Infrared thermal imaging was immediately taken when the device was removed at the 40 and 180 s. The heated skins were photographed, and the damaged area was counted after the experiment. Meanwhile, the skins after heating was cut off and utilized for hematoxylin-eosin (H&E) staining. The animal use protocol has been reviewed and approved by the Institutional Animal Care and Use Committee of the Zhejiang Center of Laboratory Animals (Approval No. ZJCLA-IACUC-20020030).

DATA AVAILABILITY

The data that support the findings of this study are available from the corresponding author upon reasonable request.

Received: 24 February 2022; Accepted: 10 May 2022;

Published online: 03 June 2022

REFERENCES

- Oh, Y. S. et al. Battery-free, wireless soft sensors for continuous multi-site measurements of pressure and temperature from patients at risk for pressure injuries. *Nat. Commun.* **12**, 5008 (2021).
- Hong, Y. J., Jeong, H. J., Cho, K. W., Lu, N. & Kim, D. H. Wearable and implantable devices for cardiovascular healthcare: from monitoring to therapy based on flexible and stretchable electronics. *Adv. Funct. Mater.* **29**, 1808247 (2019).
- Yao, S. S., Swetha, P. & Zhu, Y. Nanomaterial-enabled wearable sensors for healthcare. *Adv. Healthc. Mater.* **7**, 1700889 (2018).
- Ochoa, M. et al. Integrated sensing and delivery of oxygen for next-generation smart wound dressings. *Microsyst. Nanoeng.* **6**, 16 (2020).
- Liu, Z. et al. Integrated multiplex sensing bandage for in situ monitoring of early infected wounds. *ACS Sens.* **6**, 3112–3124 (2021).
- Liu, G. et al. Flexible drug release device powered by triboelectric nanogenerator. *Adv. Funct. Mater.* **30**, 1909886 (2020).
- Yin, M. et al. 3D printed microheater sensor-integrated, drug-encapsulated micro-needle patch system for pain management. *Adv. Healthc. Mater.* **8**, 1901170 (2019).
- Luo, H., Li, C., Shi, C., Nie, S. & Song, J. Switchable dry adhesive based on shape memory polymer with hemispherical indenters for transfer printing. *Theor. Appl. Mech. Lett.* **11**, 100308 (2021).
- Luo, H. et al. Laser-driven programmable non-contact transfer printing of objects onto arbitrary receivers via an active elastomeric microstructured stamp. *Natl Sci. Rev.* **7**, 296–304 (2020).
- Linghu, C., Zhang, S., Wang, C. & Song, J. Transfer printing techniques for flexible and stretchable inorganic electronics. *npj Flex. Electron.* **2**, 26 (2018).
- Shi, C. et al. Heterogeneous integration of rigid, soft, and liquid materials for self-healable, recyclable, and reconfigurable wearable electronics. *Sci. Adv.* **6**, eabd0202 (2020).
- Yokota, T. et al. Ultraflexible organic photonic skin. *Sci. Adv.* **2**, e1501856 (2016).
- Jeong, H. et al. Miniaturized wireless, skin-integrated sensor networks for quantifying full-body movement behaviors and vital signs in infants. *Proc. Natl Acad. Sci. USA* **118**, e2104925118 (2021).
- Wang, C. et al. Stretchable, multifunctional epidermal sensor patch for surface electromyography and strain measurements. *Adv. Intell. Syst.* **3**, 2100031 (2021).
- Wang, Y. et al. Electrically compensated, tattoo-like electrodes for epidermal electrophysiology at scale. *Sci. Adv.* **6**, eabd0996 (2020).
- Gao, W. et al. Fully integrated wearable sensor arrays for multiplexed in situ perspiration analysis. *Nature* **529**, 509–514 (2016).
- Li, H. et al. Wearable skin-like optoelectronic systems with suppression of motion artifacts for cuff-less continuous blood pressure monitor. *Natl Sci. Rev.* **7**, 849–862 (2020).
- Chen, Y. et al. Skin-like biosensor system via electrochemical channels for non-invasive blood glucose monitoring. *Sci. Adv.* **3**, e1701629 (2017).
- Jung, H. H. et al. Thin metallic heat sink for interfacial thermal management in biointegrated optoelectronic devices. *Adv. Mater. Technol.* **3**, 1800159 (2018).
- Li, H. et al. Epidermal inorganic optoelectronics for blood oxygen measurement. *Adv. Healthc. Mater.* **6**, 1601013 (2017).
- Zhan, H. et al. Biomimetic carbon tube aerogel enables super-elasticity and thermal insulation. *Chem* **5**, 1871–1882 (2019).
- Sun, K. et al. Flexible graphene aerogel-based phase change film for solar-thermal energy conversion and storage in personal thermal management applications. *Chem. Eng. J.* **419**, 129637 (2021).
- Kou, Y. et al. An intrinsically flexible phase change film for wearable thermal managements. *Energy Stor. Mater.* **34**, 508–514 (2021).
- Shi, Y., Hu, M., Xing, Y. & Li, Y. Temperature-dependent thermal and mechanical properties of flexible functional PDMS/paraffin composites. *Mater. Des.* **185**, 108219 (2020).
- Shi, J., Qin, M., Aftab, W. & Zou, R. Flexible phase change materials for thermal energy storage. *Energy Stor. Mater.* **41**, 321–342 (2021).
- Shi, J. et al. Tuning the flexibility and thermal storage capacity of solid-solid phase change materials towards wearable applications. *J. Mater. Chem. A* **8**, 20133–20140 (2020).
- Sundararajan, S., Samui, A. B. & Kulkarni, P. S. Versatility of polyethylene glycol (PEG) in designing solid-solid phase change materials (PCMs) for thermal management and their application to innovative technologies. *J. Mater. Chem. A* **5**, 18379–18396 (2017).
- Li, Y., Chen, J., Xing, Y. & Song, J. Thermal management of micro-scale inorganic light-emitting diodes on an orthotropic substrate for biointegrated applications. *Sci. Rep.* **7**, 6638 (2017).
- Shi, Y. et al. Functional soft composites as thermal protecting substrates for wearable electronics. *Adv. Funct. Mater.* **29**, 1905470 (2019).
- Jeong, S. H., Zhang, S., Hjort, K., Hilborn, J. & Wu, Z. PDMS-based elastomer tuned soft, stretchable, and sticky for epidermal electronics. *Adv. Mater.* **28**, 5830–5836 (2016).
- Silakhori, M. et al. Palmitic acid/polypyrrole composites as form-stable phase change materials for thermal energy storage. *Energy Convers. Manag.* **80**, 491–497 (2014).
- Zeng, J. et al. Myristic acid/polyaniline composites as form stable phase change materials for thermal energy storage. *Sol. Energy Mater. Sol. Cells* **114**, 136–140 (2013).
- Zhang, N. et al. A novel solid-solid phase change material: pentaglycerine/expanded graphite composite PCMs. *Adv. Eng. Mater.* **20**, 1800237 (2018).
- Xu, F., Seffen, K. A. & Lu, T. Non-fourier analysis of skin biothermomechanics. *Int. J. Heat. Mass Transf.* **51**, 2237–2259 (2008).
- Lovik, R. D., Abraham, J. P. & Sparrow, E. M. Surrogate human tissue temperatures resulting from misalignment of antenna and implant during recharging of a neuromodulation device. *Neuromodulation* **14**, 501–509 (2012).

36. Choi, S. et al. Highly conductive, stretchable and biocompatible Ag-Au core-sheath nanowire composite for wearable and implantable bioelectronics. *Nat. Nanotechnol.* **13**, 1048–1058 (2018).
37. Jung, D. et al. Highly conductive and elastic nanomembrane for skin electronics. *Science* **373**, 1022–1026 (2021).

ACKNOWLEDGEMENTS

J.S. and Y.Z. acknowledge the support of the National Natural Science Foundation of China (Grant Nos, U20A6001 and 11872331), National Key Research and Development Program of China (Grant No, 2019YFE0117400), and Zhejiang University K.P. Chao's High Technology Development Foundation.

AUTHOR CONTRIBUTIONS

S.N., M.C., and H.Y. contributed equally to this work. S.N., M.C., and J.S. conceived the ideas and designed the experiments. S.N., M.C., H.Y., L.S., and S.W. performed experiments. S.N., Y.Z., and J.S. wrote the manuscript.

COMPETING INTERESTS

The authors declare no competing interests.

ADDITIONAL INFORMATION

Supplementary information The online version contains supplementary material available at <https://doi.org/10.1038/s41528-022-00174-8>.

Correspondence and requests for materials should be addressed to Yang Zhu or Jizhou Song.

Reprints and permission information is available at <http://www.nature.com/reprints>

Publisher's note Springer Nature remains neutral with regard to jurisdictional claims in published maps and institutional affiliations.



Open Access This article is licensed under a Creative Commons Attribution 4.0 International License, which permits use, sharing, adaptation, distribution and reproduction in any medium or format, as long as you give appropriate credit to the original author(s) and the source, provide a link to the Creative Commons license, and indicate if changes were made. The images or other third party material in this article are included in the article's Creative Commons license, unless indicated otherwise in a credit line to the material. If material is not included in the article's Creative Commons license and your intended use is not permitted by statutory regulation or exceeds the permitted use, you will need to obtain permission directly from the copyright holder. To view a copy of this license, visit <http://creativecommons.org/licenses/by/4.0/>.

© The Author(s) 2022